Supporting Information

How to Make an Efficient Gas-Phase Heterogeneous CO_2 Hydrogenation Photocatalyst

Tingjiang Yan, Na Li, Lilin Wang, Qin Liu, Feysal M. Ali, Lu Wang, Yangfan Xu, Yan Liang, Ying Dai, Baibiao Huang, Jinmao You*, Geoffrey A. Ozin**

Synthesis of InOOH precursor and $In_2O_{3-x}(OH)_y$ All reagents were used as received. N,N-dimethylformamide (DMF), Indium(III) nitrate hydrate ($In(NO_3)_3$•$4.5H_2O$, In 99.9%) and ethanol (C_2H_5OH) were purchased from Sigma-Aldrich. Deionized water was used throughout the synthesis. In a typical synthesis, 0.3 g of $In(NO_3)_3$•$4.5H_2O$ was dissolved in a mixed DMF/H_2O solution (16.2 mL / 0.8 mL) under magnetic stirring for 30 min to form a homogeneous solution. The aqueous solution was transferred into a Teflon-lined stainless autoclave and then heated at 150 °C for 24 hours. After being cooled to room temperature, the white products were collected through centrifugation, washed with ethanol and water, and finally dried at 60 °C in vacuum. The dried InOOH precursors were then placed into a tubular furnace and gradually annealed with the ramp rate of 10 °C min^{-1} to various temperatures (390-450 °C) and kept for 4 hours under air condition to obtain the final $In_2O_{3-x}(OH)_y$ samples.

Material characterizations Powder X-ray diffraction (PXRD) was performed on a Bruker D2-Phaser X-ray diffractometer, using Cu Kα radiation at 30 kV. Raman spectra were obtained using a SENTERRA Raman spectrometer (Bruker), excited by a He-Ne laser with a wavelength of 532 nm. Differential scanning calorimetric (DSC) and thermogravimetric analysis (TG) were carried out with a NETZSCH STA-449C simultaneous apparatus with a heating rate of 10 °C min^{-1} in flowing air. The transmission electron microscopy (TEM) measurement was conducted using a JEM–2010 microscope working at 200 kV. Samples for

Operando high-resolution transmission electron microscopy (HRTEM) were treated in N_2 atmosphere at 120 ° C for 10 min and then switched into air condition to collect at different annealing temperatures. Nitrogen Brunauer-Emmet-Teller (BET) adsorption isotherms were obtained using an ASAP2020 M apparatus (Micrometrics Instrument Corp., USA). For BET surface area analyses, the samples were degassed in vacuum at 110 °C for 10 h and then measured at 77 K. UV-visible diffuse reflectance spectra (DRS) of the powders were obtained for the dry-pressed disk samples using a Cary 500 Scan Spectrophotometer (Varian, USA) over a range of 200–800 nm. $BaSO_4$ was used as a reflectance standard in the UV-visible diffuse reflectance experiment. X-ray photoelectron spectroscopy (XPS) was performed using a PerkinElmer Phi 5500 ESCA spectrometer in an ultrahigh vacuum chamber with a base pressure of 1×10^{-9} Torr. The spectrometer uses an Al Kα X-ray source operating at 15 kV and 27 A. The samples were coated onto carbon tape, and all results were calibrated to C1s 284.5 eV. The photoluminescence (PL) spectra was measured on an Andor Shamrock SR-750 fluorescence spectrometer with a Xe-lamp as an excitation source (Andor Technology Ltd, Belfast, UK). A CCD detector combined with a monochromator was used for signal collection. The sample was filled in an iron sample cell and the temperature of the sample was increased from 298 to 543 K heated by resistive wire elements. A copper-constant thermocouple buried in the sample was used to monitor the sample's temperature with a measurement error of ±1.5 K. The static surface photovoltage (SPV) measurements were performed under ambient conditions by by a lock-in amplier (SR830) synchronized with a light chopper (SR540). The monochromatic light was obtained by passing light from a 500W Xenon lamp (CHF XQ500 W) through a double prism monochromator (SBP300). The photovoltage cell is mainly consisting of two ITO quartz glass electrodes and the powder sample sandwiched between the two ITO quartz glass electrodes. Theoretical calculations are carried out using density functional theory (DFT), as implemented in the Vienna ab initio simulation package with

projector augmented-wave (PAW) pseudopotentials within the generalized gradient approximations (GGA).[1,2] The cutoff energy for the plane-wave is set to 500 eV, and the convergence tolerance for energy is 10^{-5} eV. All structures were relaxed until the force is less than 0.01 eV $Å^{-1}$. To model the surfaces, four-layer slabs are adopted with the bottom two layers keep fixed.

The in-situ photo-deposition experiments were performed by using $HAuCl_4$ and $MnSO_4$ as precursors. For photo-reduction of Au(III) to Au nanoparticles, 50 mg polymorphic heterostructure $In_2O_{3-x}(OH)_y$ sample (T405) and $HAuCl_4$ precursor (Au mass is 0.5 wt% of $In_2O_{3-x}(OH)_y$ amount) were added into 100 mL aqueous methanol solution (10 vol%) under magnetic stirring and the resultant suspension was irradiated by an unfiltered 300 W Xe lamp (PLS-SXE300D, Beijing Perfectlight Technology Co., Ltd) for 0.5 h. For photo-oxidation of Mn(II) to Mn_2O_3 nanoparticles, the $In_2O_{3-x}(OH)_y$ sample (T405, 50 mg) and $MnSO_4$ precursor ($MnSO_4$ mass is 1 wt% of $In_2O_{3-x}(OH)_y$ amount) were added into 100 mL aqueous $NaIO_3$ solution (5 mM) under magnetic stirring and the resultant suspension was irradiated by an unfiltered 300 W Xe lamp (PLS-SXE300D, Beijing Perfectlight Technology Co., Ltd) for 4 h. The solids obtained from the photo-reduction and photo-oxidation reactions were collected through centrifugation, washed with ethanol and water, and finally dried at 80 °C in vacuum.

Gas phase CO_2 hydrogenation tests Photocatalytic gaseous CO_2 hydrogenation experiments were performed in a flow reactor using tubular quartz with an inner diameter of 2 mm, In brief, ~ 15 mg of catalyst was packed into the tubular quartz and fully irradiated with an unfiltered 130 W Xe lamp. The diameter of the light spot was about 2 cm, with an area of about 3.14 cm^2, ensuring the full cover of the sample. An OMEGA temperature controller was attached to a heating cartridge inserted into the copper block along with a thermocouple inserted into the quartz tube in contact with the catalyst bed for control of the catalyst

temperature at 270 °C. CO_2 and H_2 with a ratio of 1 : 3 (0.5 sccm and 1.5 sccm) were introduced into the reactor by Alicat Scientific digital flow controllers. The amounts of CO and CH_3OH produced were analyzed by an on-line gas chromatograph (Agilent 7820A), equipped with a thermal conductivity detector (TCD) and a flame ionization detector (FID).

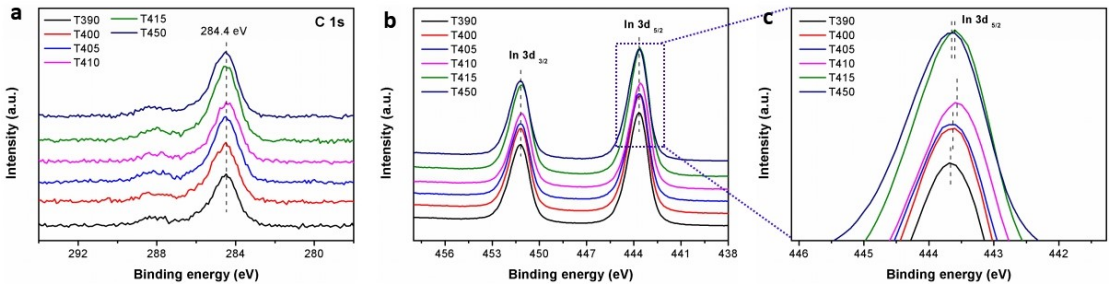

Fig. S1 XPS spectra of (a) C 1s, (b, c) In $3d_{5/2}$ and In $3d_{3/2}$ core level of various $In_2O_{3-x}(OH)_y$ samples.

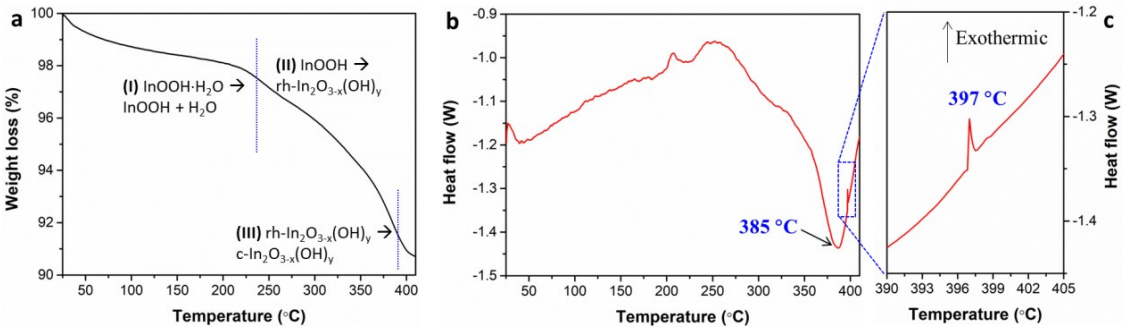

Fig. S2 TG-DSC plots of the InOOH precursor in the temperature range 25-410 °C at a ramp rate of 10 °C min^{-1}: a) TG. b) and c) DSC.

The dehydroxylation of the InOOH precursor and phase transformation from rhombohedral to cubic phase was tested using thermogravimetric (TG) and differential scanning calorimeter (DSC) analysis. The TG curve can be divided into three typical weight loss steps. The first step (I) in the range of 25-240 °C can be attributed to the physisorbed-chemisorbed water loss and the residual DMF removal from the precursor. A sharp weight loss is observed in the second step from 240 to 390 °C, accompanied by an endothermic peak at ~385 °C, corresponds to the conversion of InOOH into rh-$In_2O_{3-x}(OH)_y$ through

dehydroxylation of the hydroxyl groups. The total weight loss for this step is 5.93 %, which is very close to the calculated theortical loss (6.08 %). Furthermore, an obvious exothermic peak at ~397 °C in the third set is seen (III) between 390-410 °C, which is associated with the phase transformation from rh-$In_2O_{3-x}(OH)_y$ to c-$In_2O_{3-x}(OH)_y$.

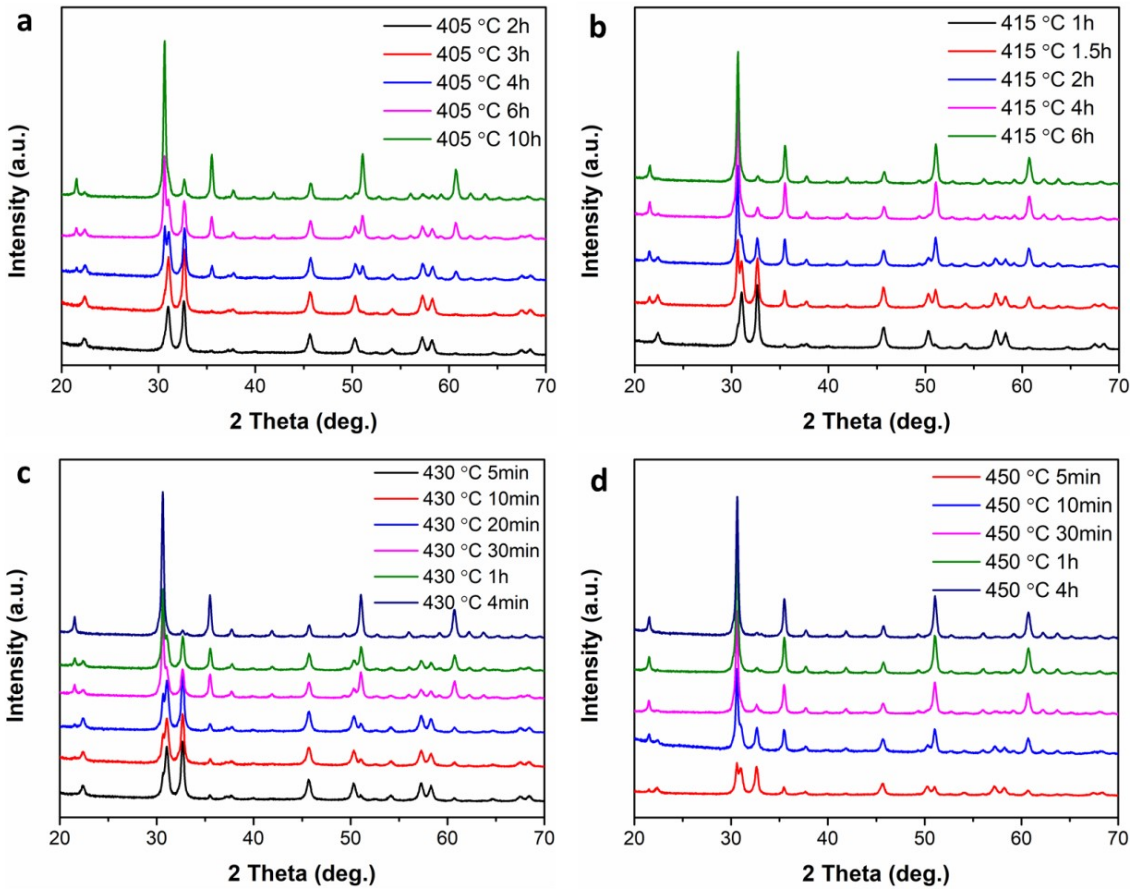

Fig. S3 PXRD patterns of the samples annealed at four typical temperatures for different reaction times. a) 405 °C. b) 415°C. c) 430 °C. d) 450 °C.

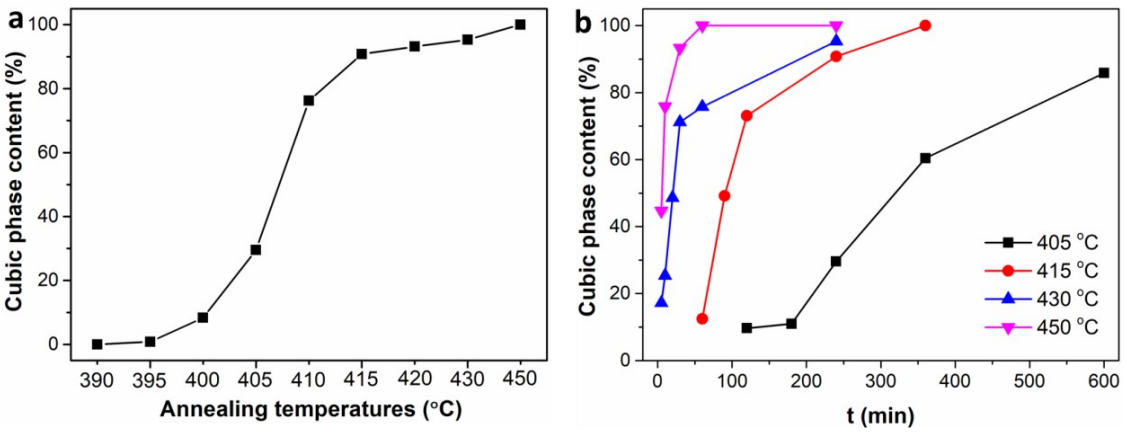

Fig. S4 Dependence of cubic $In_2O_{3-x}(OH)_y$ content of samples on the a) annealing temperatures and b) reaction times.

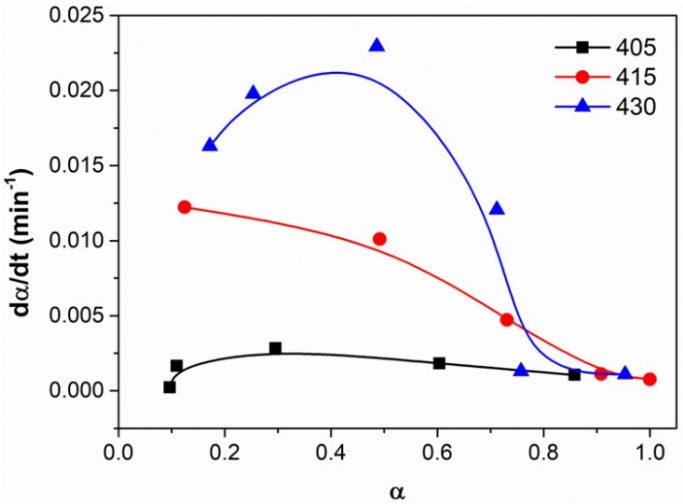

Fig. S5 Rate of formation of the cubic $In_2O_{3-x}(OH)_y$ phase as a function of α (phase content) at different temperatures.

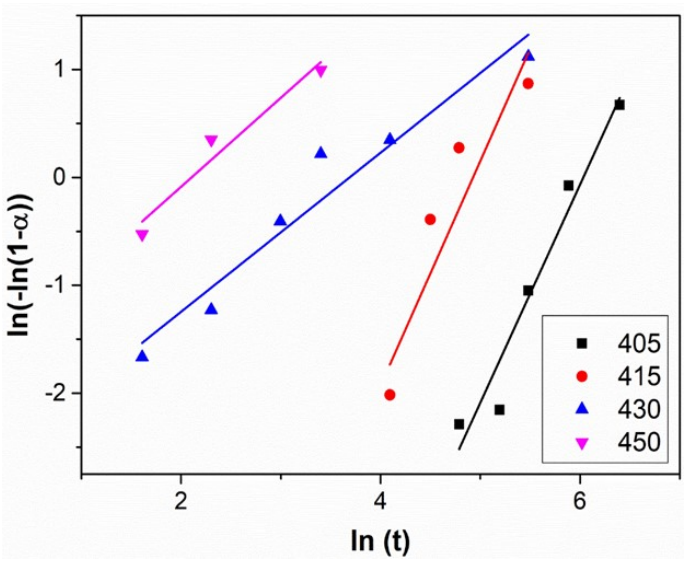

Fig. S6 JMAEK equation linear fit for different fractions of the cubic $In_2O_{3-x}(OH)_y$ phase.

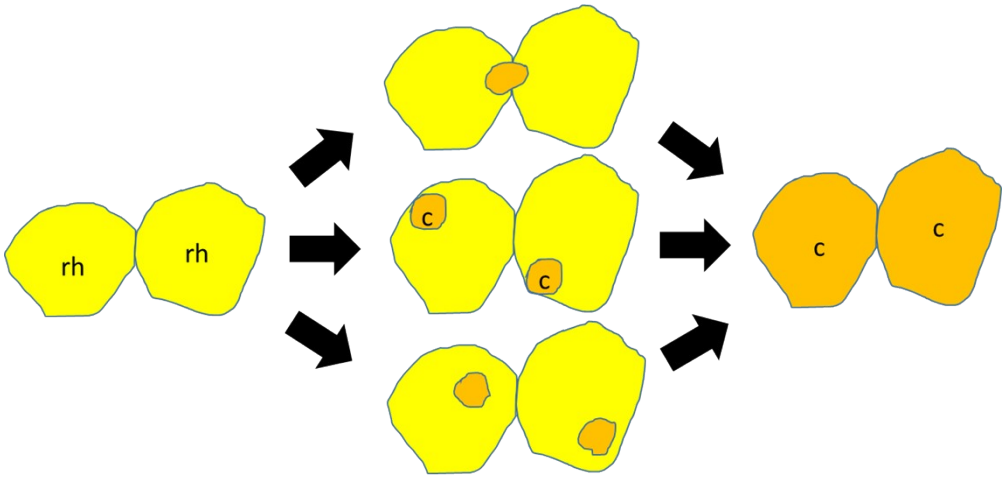

Fig. S7 Schematic cartoon of three possible nucleation and growth models for the phase transformation from rh- to c-$In_2O_{3-x}(OH)_y$ nanocrystals: interface nucleation (top), surface nucleation (middle), and volume nucleation (bottom).

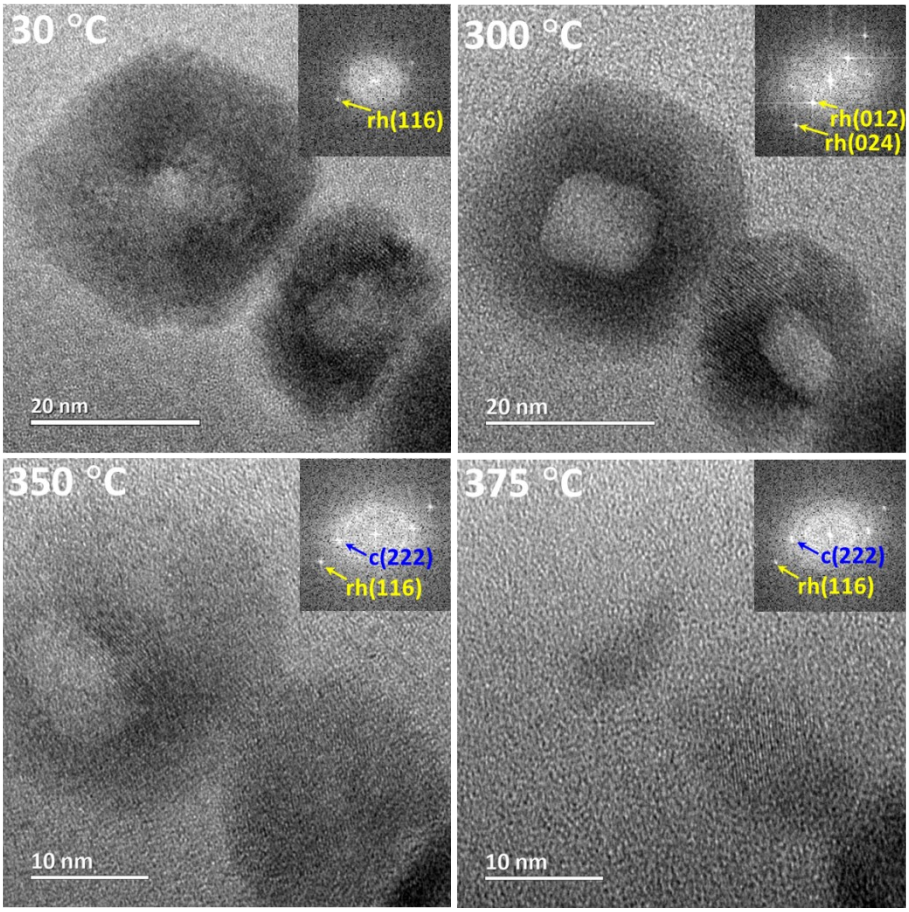

Fig. S8 *Operando* HRTEM of rh-$In_2O_{3-x}(OH)_y$ (pre-treated at 350 °C) and thermally annealed samples in air at different temperatures. The colored number in the SAED patterns represents different crytsal phases, yellow: rh-$In_2O_{3-x}(OH)_y$; blue: c-$In_2O_{3-x}(OH)_y$.

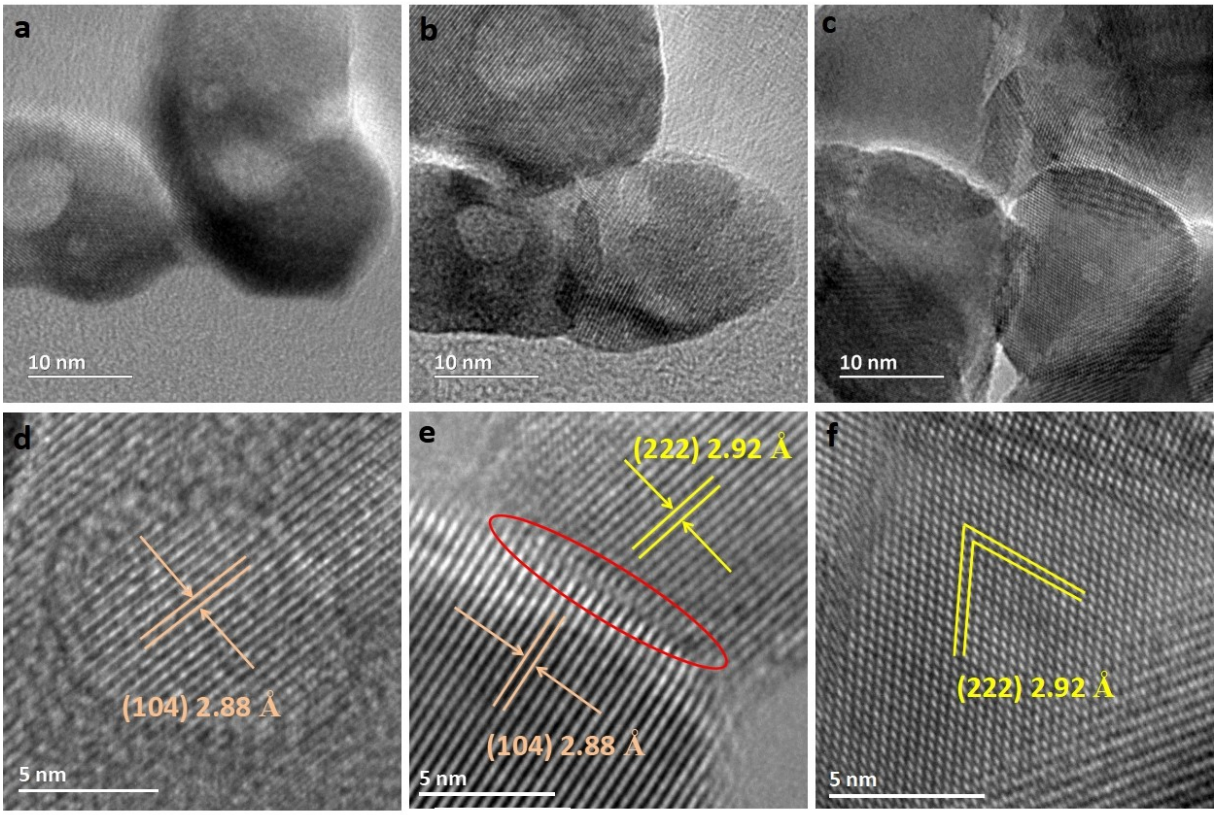

Fig. S9 TEM images of various $In_2O_{3-x}(OH)_y$. a) and d) Pure rh-$In_2O_{3-x}(OH)_y$, T390. b) and e) rh/c-$In_2O_{3-x}(OH)_y$, T405, c) and f) Pure c-$In_2O_{3-x}(OH)_y$, T450.

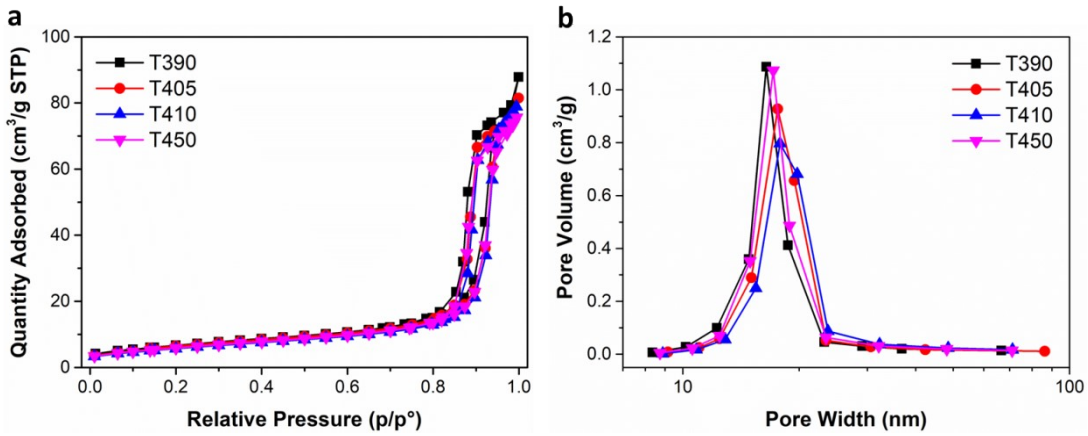

Fig. S10 a) N_2 physisorption isotherms and b) pore size distributions of various $In_2O_{3-x}(OH)_y$ samples.

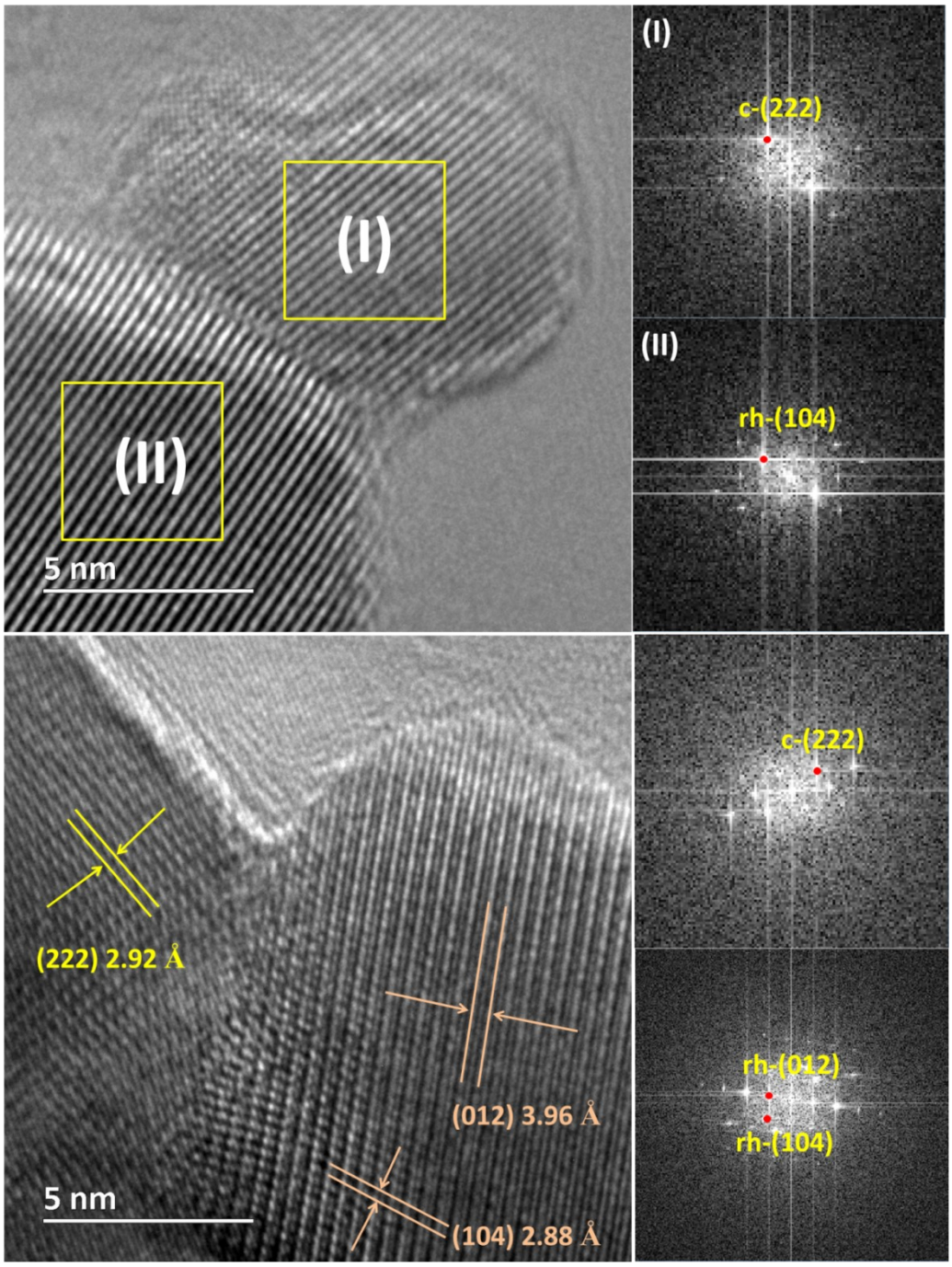

Fig. S11 TEM images and FFTs of rh/c-$In_2O_{3-x}(OH)_y$ (T405).

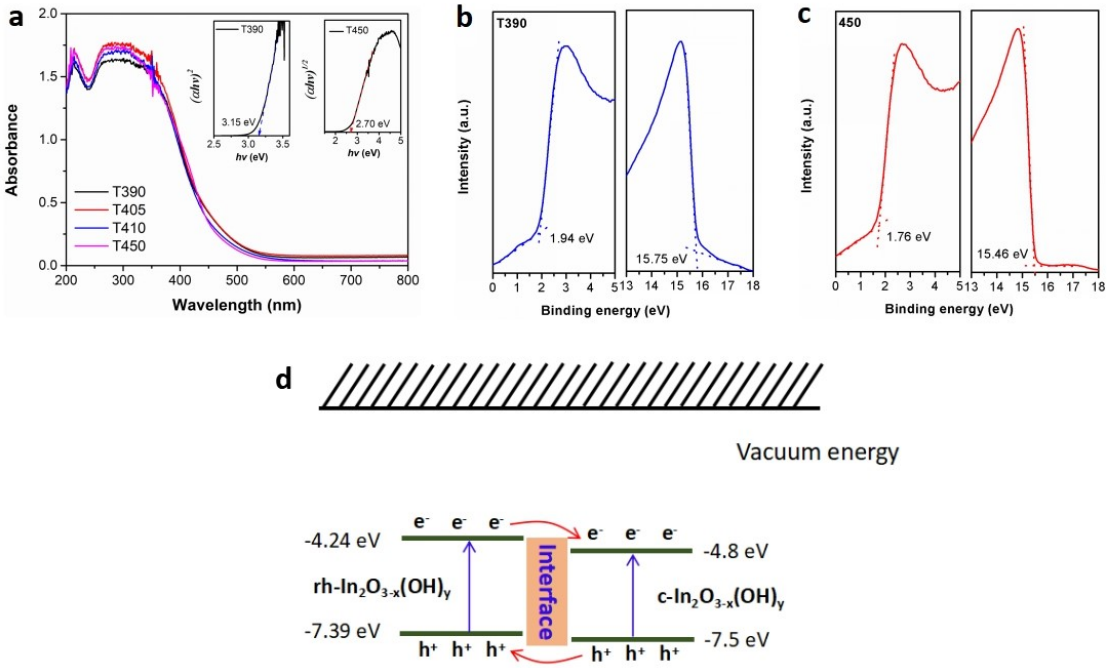

Fig. S12 a) UV-vis DRS spectra of the as-prepared $In_2O_{3-x}(OH)_y$ samples. Insets are the band gap energy of pure rh-$In_2O_{3-x}(OH)_y$ (T390) and c-$In_2O_{3-x}(OH)_y$ (T450). b) UPS spectra of rh-$In_2O_{3-x}(OH)_y$ (T390). c) UPS spectra of c-$In_2O_{3-x}(OH)_y$ (T450). d) Position of the energy levels of the conduction band (CB) edge and the valence band (VB) edge of rh-$In_2O_{3-x}(OH)_y$ and c-$In_2O_{3-x}(OH)_y$ with respect to the absolute vacuum energy scale (AVS). UPS is a useful technique to establish the VB energy for semiconductors. The VB versus Fermi level and the end energy level (EEL) for pure rh-$In_2O_{3-x}(OH)_y$ (T390) are determined to be ca. 1.94eV and 15.75 eV by fitting a straight line to the leading edge, respectively. The work function (ϕ) can be calculated to be ca. 5.45 eV according to the equation $\phi = 21.2 - EEL$. Thus the the E_{VB} (vs vaccum) is –7.39 eV and the E_{CB} (vs vacuum) is -4.24 eV as determined from the band gap energy in the UV-vis DRS. Accordingly, the E_{VB} (vs vacuum) and the E_{CB} (vs vacuum) for pure c-$In_2O_{3-x}(OH)_y$ (T450) are –7.5 eV and -4.8 eV, respectively.

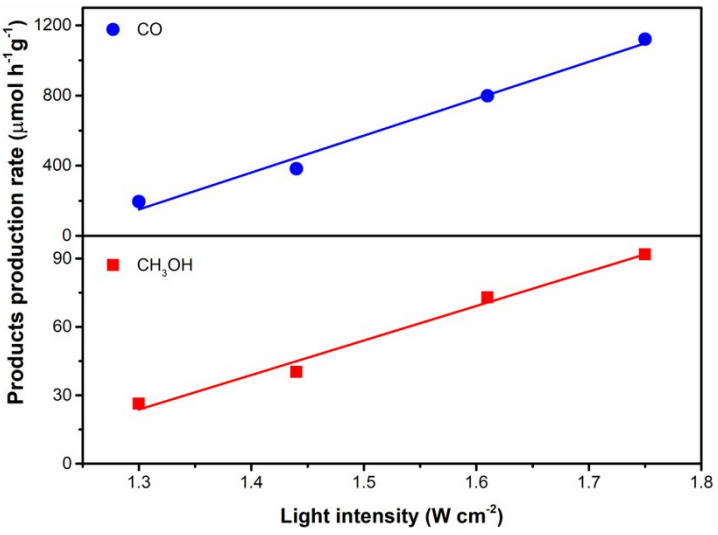

Fig. S13 Effect of light intensity on the CH_3OH and CO production rate of rh/c-$In_2O_{3-x}(OH)_y$ (T405) under irradiation from a 130 W Xe lamp at different light intensities.

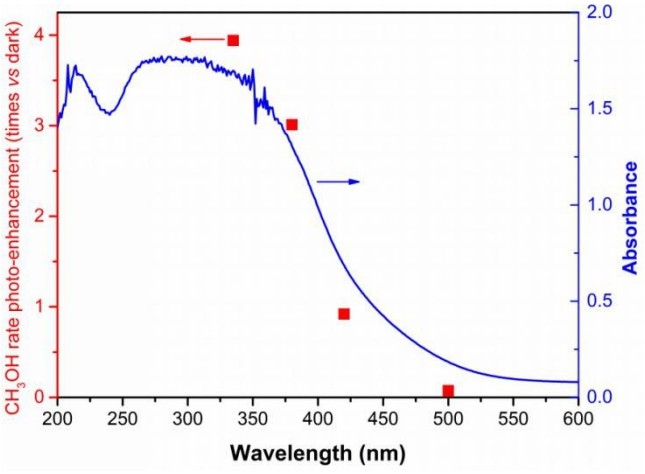

Fig. S14 Wavelength dependence of the photocatalytic CH_3OH rate enhancement on rh/c-$In_2O_{3-x}(OH)_y$ (T405) upon light irradiation with cut-off filters of different wavelengths (with respect to dark condition at 270 °C), a kind of photo activity spectrum. The intensity of the irradiated light at all wavelengths was kept to about 1.75 W cm^{-2}.

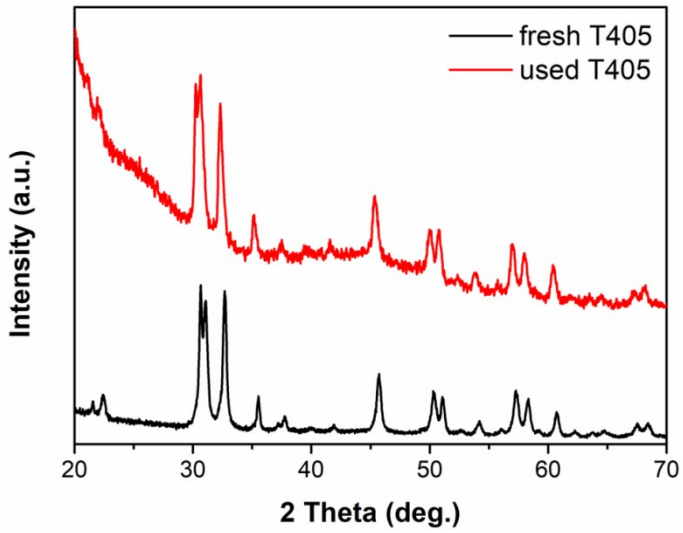

Fig. S15 PXRD patterns of the rh/c-$In_2O_{3-x}(OH)_y$ sample (T405) before and after the 50 h long-term stability test.

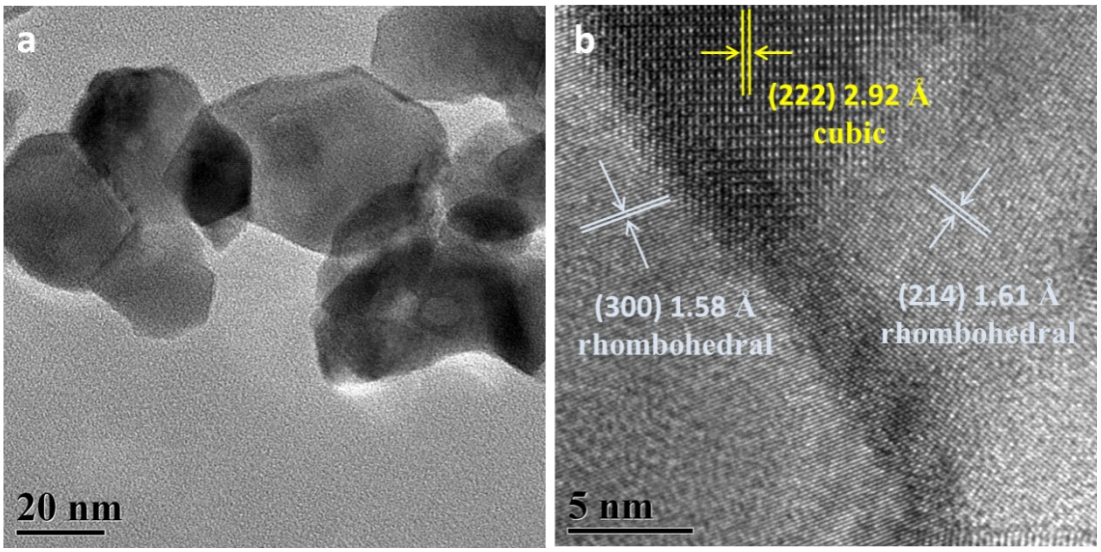

Fig. S16 a) TEM and b) HRTEM images of the spent rh/c-$In_2O_{3-x}(OH)_y$ sample (T405) after the 50 h long-term stability test.

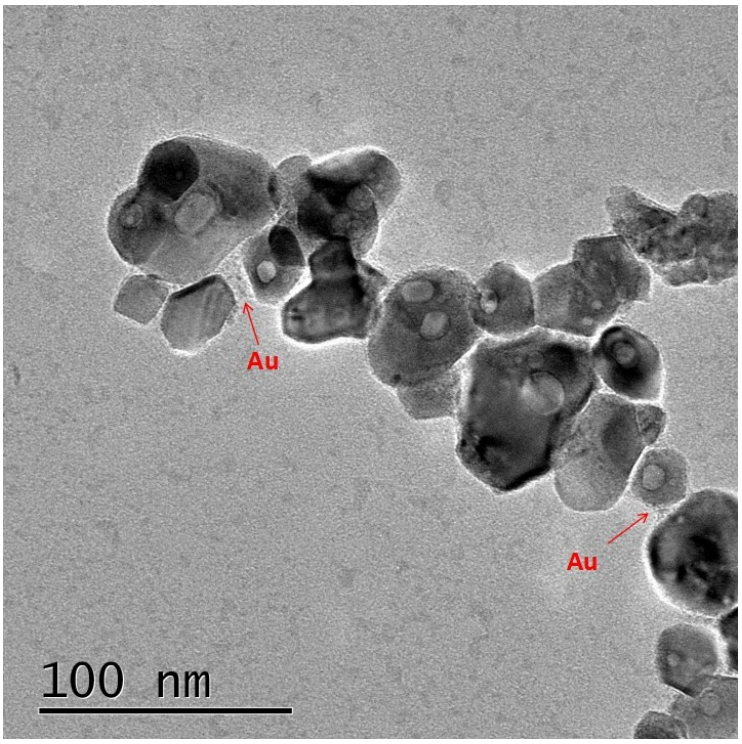

Fig. S17 TEM image of rh/c-$In_2O_{3-x}(OH)_y$ sample (T405) after in-situ photo-reduction of Au(III) to Au nanoparticles.

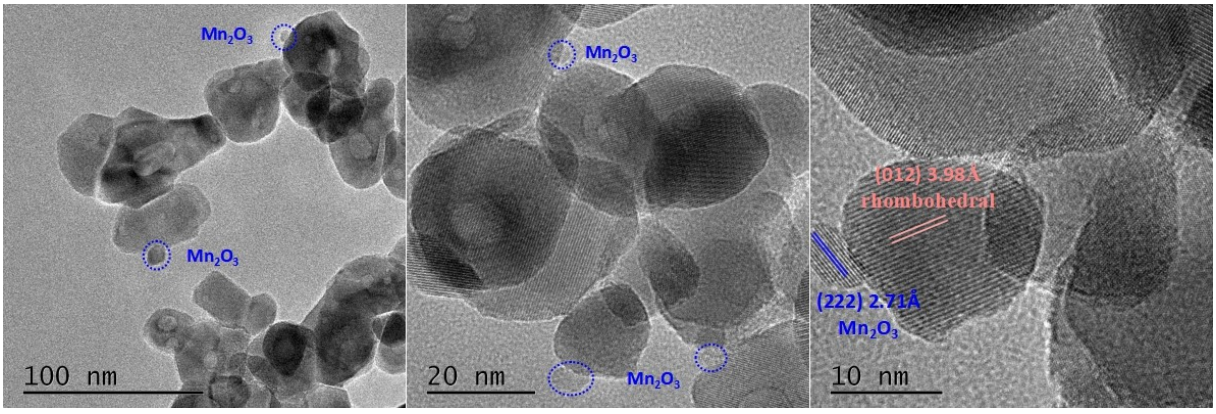

Fig. S18 TEM images of the rh/c-$In_2O_{3-x}(OH)_y$ sample (T405) after in-situ photo-oxidation of Mn(II) to Mn_2O_3 nanoparticles.

Table S1 Values of *n* and *k* obtained from the JMAEK plot.

T (°C)	n	k (min^{-1})
405	2.02	0.0024
415	1.93	0.0069
430	0.74	0.0253
450	0.82	10.12

Table S2 Specific surface area, pore size and pore volume of the obtained $In_2O_{3-x}(OH)_y$ samples.

Samples	Specific surface area ($m^2\ g^{-1}$)	Pore size (nm)	Pore volume ($cm^3\ g^{-1}$)
T390	24.2	17.2	0.123
T405	22.5	18.3	0.119
T415	21.2	19.3	0.118
T450	22.1	17.8	0.114

Table S3 The ratio of oxygen vacancies ([O]) and hydroxide groups (OH) in the polymorphic heterostructures of rh/c-$In_2O_{3-x}(OH)_y$. The concentrations of [O] and OH are calculated from XPS.

rh/c-$In_2O_{3-x}(OH)_y$	[O] (at. %)	OH (at. %)	Ratio of [O]/OH
T390	23.23	7.11	3.26
T400	30.56	6.57	4.65
T405	32.36	5.75	5.62
T410	33.14	4.67	7.09
T415	31.66	4.13	7.66
T450	31.19	3.75	8.31

References

1. G. Kresse, D. Joubert, *Phys. Rev. B* **1999**, *59*, 1758-1775.

2. J. P. Perdew, K. Burke, Y. Wang, *Phys. Rev. B* **1996**, *54*, 16533−16539.